Advances in Science and Technology Research Journal

Advances in Science and Technology Research Journal, 2026, 20(5), 103–114
https://doi.org/10.12913/22998624/215487
ISSN 2299-8624, License CC-BY 4.0

Received: 2025.11.20
Accepted: 2026.03.15
Published: 2026.04.01

Analysis of selected tribological properties of cellulose products in the context of process disruptions in packaging and sorting machines

Kamil Kurpanik[1*], Tomasz Machoczek[1], Paweł Jureczko[1], Tomasz Rusin[2], Wojciech Pakieła[3]

[1] Department of Theoretical and Applied Mechanics, Faculty of Mechanical Engineering Technology, Silesian University of Technology, Konarskiego 18A, 44-100 Gliwice, Poland
[2] Dantec Dynamics GmbH, Kässbohrer Str. 18, D 89077 Ulm, Germany
[3] Departament of engineering Materials and Biomaterials, Faculty of Mechanical Engineering, Silesian University of Technology, Akademicka Str. 2A, 44-100 Gliwice, Poland
* Corresponding author's e-mail: kamil.kurpanik@polsl.pl

ABSTRACT

Cigarette production is a highly automated process in which friction between fibrous materials plays a key role in the handling, transport, and packaging of tobacco products. Excessive friction often leads to sorting slot blockages and production line downtime, highlighting clear economic relevance. This study examined the tribological behaviour of selected cigarette types, focusing on the interaction between cigarette tube material and the anodised aluminium track of the transport and sorting machine. Experimental research combined classic surface roughness measurements with the optical digital image correlation (DIC) method, ensuring high accuracy and repeatability under controlled environmental conditions. The average static friction coefficient was found to be 0.28, with noticeable differences observed between sample groups taken from different cigarette packs, as characterised later in the study. Moreover, the developed DIC-based setup proved effective for analysing subtle tribological interactions. These findings provide quantitative insights into material performance and offer practical guidance for reducing friction-related production issues within the tobacco industry.

Keywords: tribology, cellulose fibres, cigarette filters, surface roughness, digital image correlation, porous nonwovens.

INTRODUCTION

Friction and tribological properties of fibrous materials play a significant role in shaping their mechanical properties, durability and functionality [1,2]. In the context of mass production of tobacco products, friction mechanisms are particularly important, as the transport, sorting and handling of finished cigarettes are susceptible to disruptions resulting from excessive friction resistance. These interactions can occur both between cigarette paper, filters and machine components, and between the products themselves during handling, leading to blockages, production line instability, downtime and losses [3]. The intensity of friction in fibrous materials depends on a number of factors, such as fibre microstructure, contact geometry, material composition and environmental conditions [1,2]. The contact morphology – including the differences between point and line contact – in combination with the mechanical properties of the fibre contact area strongly determines the friction resistance. The shape of the fibre cross-section, the degree of molecular orientation, the use of heat treatment and the type of fibre can significantly change the coefficient of friction. For example, fibres with a circular cross-section and high molecular orientation exhibit increased values of this parameter [1]. The tribological behaviour of fibrous materials depends

largely on environmental conditions, particularly humidity and temperature. Changes in humidity affect surface energy, adsorption layers and fibre deformation, leading to varying friction responses. Increased humidity usually reduces the coefficient of friction by forming thin water films with lubricating properties, although in some cases it promotes fibre swelling and increased wear [4, 5, 6]. Water often acts as a natural lubricant, reducing friction by forming protective layers, especially in hydrophilic materials [7, 8]. However, this effect is not universal – in selected fibre-reinforced polymers, a humid environment reduces wear by removing abrasion products and providing a cooling effect, while in others it leads to plasticisation of the matrix and abrasive wear [8, 9, 10]. In addition, the microstructural texture and orientation of the fibres significantly affect wear resistance. Texturing improves wear resistance in dry conditions, but in a humid environment it can increase water absorption and wear intensity [9, 11]. Another important factor is the formation of tribological films (tribo-films), which reduce friction but often lose their cohesion at high humidity and do not provide lasting surface protection [12].

In fibrous structures such as mats or cigarette papers, friction and adhesion between fibres are the main mechanisms responsible for energy dissipation during mechanical deformation [13,14]. The behaviour of the system includes elastic stages, slip with strengthening and stiffening, with friction playing a key role in the transition between these states. At the microscopic level, the frictional resistance between individual fibres depends on the prestress and elastic deformation at the point of contact, with elastic deformation being more important than the fibre braid [15]. Importantly, friction between oriented fibres can take on a solid-like character and increase logarithmically with sliding speed, indicating complex, non-linear interaction mechanisms.

Modifications to the surface of fibres, such as the use of polymer brushes, can lead to a significant reduction in friction resistance and the introduction of a regime resembling liquid flow (Stokes resistance) [3]. Friction in fibrous materials is often modelled empirically using relationships of the type F, where the parameters a and n depend on the structural properties of the material and the contact conditions, allowing the non-linear and hysteretic nature of friction to be captured, especially under low stress conditions [1,16]. In the case of tobacco products, an in-depth analysis of these mechanisms enables the optimisation of cigarette transport and sorting processes, minimising downtime and production losses [17,18].

In the tobacco industry, the problem of friction in fibrous materials is particularly important, especially in the context of cigarette packaging machines. As shown in Figure 1, these devices are characterised by complex transport track geometry and the interaction of many mechanical components, which creates numerous points of contact between the products and the machine elements. It is these contacts that are the source of instability and production downtime resulting from excessive frictional resistance. Due to

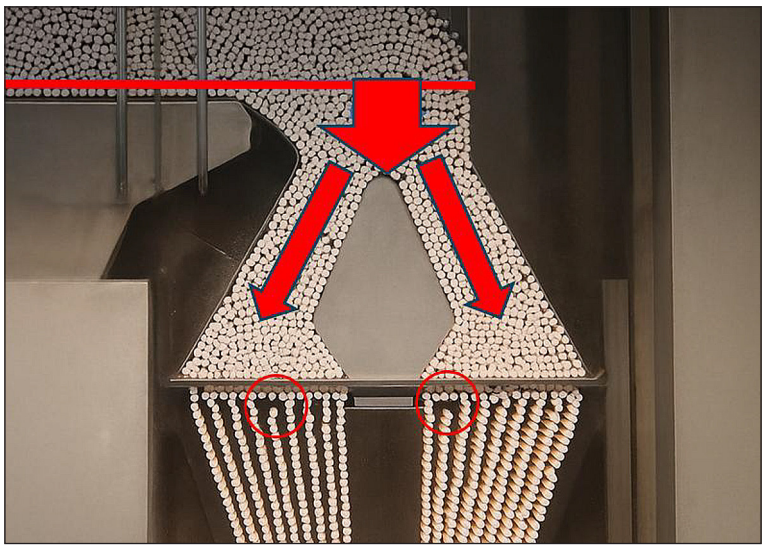

Figure 1. Fragment of a cigarette sorting machine

the practical significance of this phenomenon, an attempt was made to analyse it in detail with the aim of quantitatively and qualitatively characterising the friction mechanisms within finished cigarettes. At the same time, this issue poses a scientific challenge, as friction resistance in fibrous products is the result of complex microscopic and macroscopic interactions, and their modelling requires consideration of numerous structural, environmental and operational factors.

Figure 2 shows a close-up of the conveyor belt used to transport the finished product, on which the spaces blocked by the items - cigarettes - are clearly visible. This observation highlights the practical effects of friction resistance in the production process, while also providing motivation to analyse the tribological properties of materials used in cigarette products. These properties – including friction and surface interactions – are critical to production efficiency, especially at the sorting stage, mechanical durability and environmental impact.

Although direct tribological studies of tobacco products are not widely reported in the literature, numerous studies provide information on the structure, morphology and mechanical properties of various tobacco products, which are closely related to their tribological behaviour.

In the context of industrial friction analysis of fibrous materials, particularly in cigarette packaging machines, it is essential to use precise and non-contact measurement methods. Digital image correlation is such a technique, widely used to assess displacements, deformations and the behaviour of materials under load [19,20]. This method enables the generation of full-field, high-resolution measurement data, which makes it particularly useful in materials research and structural diagnostics [19,21,22]. DIC allows the tracking of characteristic patterns on the sample surface applied for research purposes, eliminating the need for contact strain gauges and simplifying the experimental setup [21–23]. In addition, this technique enables real-time monitoring of crack propagation, including through crack opening measurement (CMOD) and crack tip location [23–26]. Modern DIC systems, equipped with automation and advanced image processing, allow for the analysis of deformations in a wide field of view and the detection of defects invisible to the naked eye, thus increasing the accuracy and reliability of measurements [22,25,27–29].

In summary, the tribological properties of fibrous materials, including those used in tobacco products, are determined by structural and environmental factors such as fibre microstructure, cross-sectional geometry, humidity and ambient temperature. Literature studies show that surface modifications, the use of lubricating coatings or nanostructural reinforcement can significantly reduce friction resistance and wear [1,2,13,16,30–33].

Due to the specific shape and subtle mass of the analysed samples, classical research methods prove to be insufficient. Therefore, the aim of this work is to develop an innovative research methodology for the analysis of the tribological properties of cellulose-based fibrous products used in the tobacco industry under conditions corresponding to actual production processes (temperature from 20 to 24 °C, relative air humidity 55–75%) [16].

The research used profilometry and the optical technique of digital image correlation, which allowed data to be obtained on both a micro and macro scale, enabling detailed characterisation of displacements, deformations and the behaviour of materials during movement.

MATERIALS AND METHODS

The study used a statistical population of finished industrial cigarettes, which were placed on a treadmill made of anodised aluminium, reflecting a fragment of the transport and sorting system

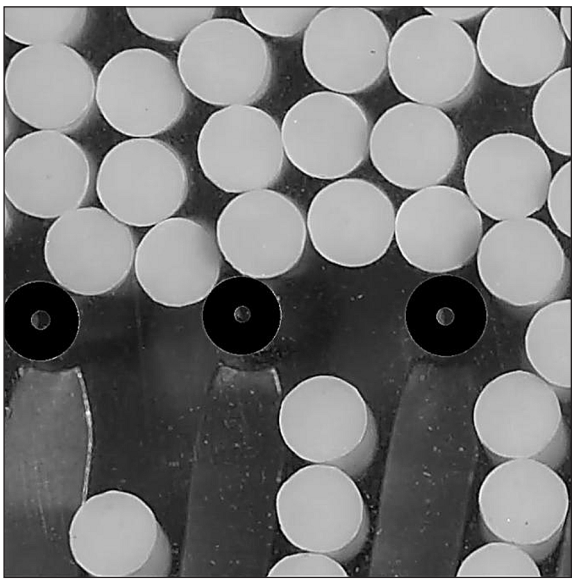

Figure 2. Transport track for finished products. View of empty spaces indicating a break in the transport process

used in production processes. This solution made it possible to accurately reproduce industrial conditions and take into account the impact of the conveyor belt surface properties on friction mechanisms and interactions between products. Before the measurements were taken, the samples were conditioned at a controlled temperature and humidity, which ensured the repeatability and comparability of the results and minimised the impact of factors interfering with the friction process, such as moisture absorption or deformation resulting from environmental differences. In order to better characterise the components assembled in the experiment, tests were carried out to identify the roughness of specific contact surfaces.

Materials

A population of 100 samples consisting of Chesterfield cigarettes (Figure 3) from 5 different packs was used in the tests to determine the surface characteristics.

For the purposes of the study, the structure and geometry of the cigarette samples were analysed and the surface structure of both the filter tube and the part containing the tobacco mixture was identified (Figure 4). To this end, the cigarette papers of the tested cigarettes were cut open and unrolled, and then attached to flat, degreased aluminium plates using double-sided adhesive tape (Figure 5).

The tests were performed using a VK-X3100 optical profilometer (KEYENCE CORPORATION, Japan), which enables non-destructive, three-dimensional analysis of surface topography with an image resolution of 1024 × 768 px (Figure 6). Thanks to the analysis of interference fringes and signal interpolation, the device achieves a vertical resolution of 0.1 nm, which allows for precise recording of height differences on a nanometric scale. The obtained topography maps were used to assess the homogeneity and stability of the tribological properties of the tested cigarette paper surfaces and the treadmill during the tests.

Figure 3. Structure of the tested samples

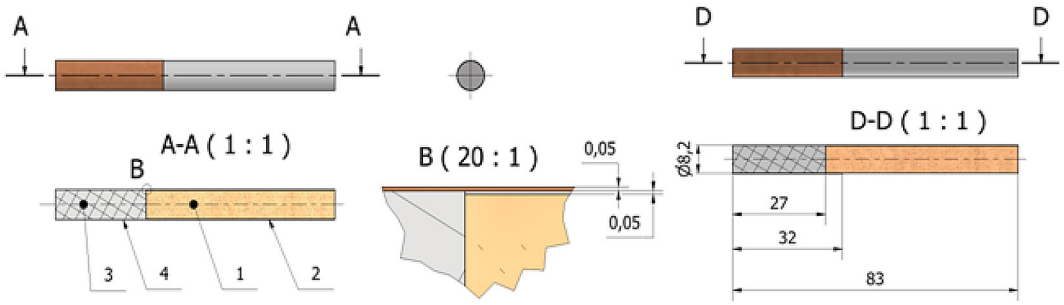

Figure 4. Cross-section and geometric dimensions of the tested samples, where: 1 – tobacco mixture (70.13% of the cigarette weight), 2 – tube for tobacco mixture (6.49%), 3 – filter (15.59%), 4 – filter tube (7.79%)

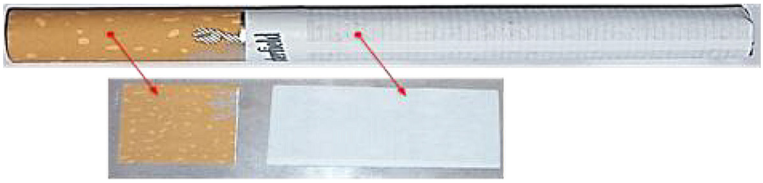

Figure 5. View of a sample of tissue paper, unfolded and attached to a flat surface for the purposes of profilometric testing

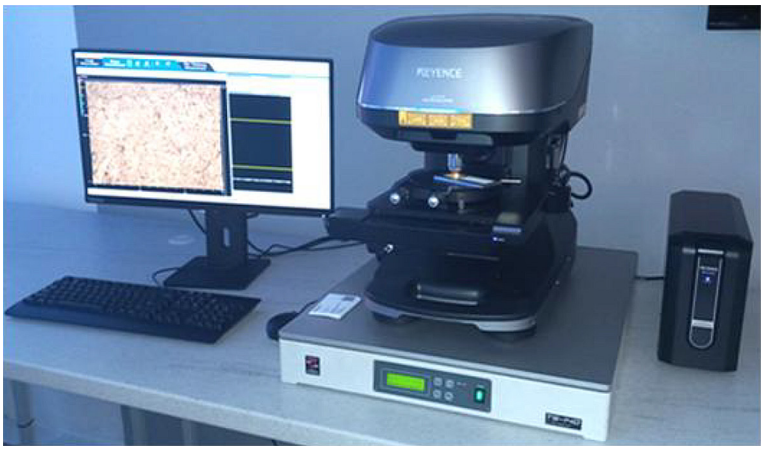

Figure 6. VK-3100 optical profilometer during cigarette tube roughness testing

The measurement covered a range of standard surface topography parameters, such as arithmetic mean roughness Ra and profile height Rz, enabling a comprehensive assessment of the microgeometry of the outer surface of the paper samples tested. The measurement procedure was carried out in accordance with applicable ISO standards, including ISO 4287 and ISO 4288, ISO 3274 and ISO 11562, which ensured the comparability and repeatability of the results. The data obtained (Figure 7) enabled a thorough analysis of the impact of the tread topography on friction and contact interactions with the tested products, constituting an important element in

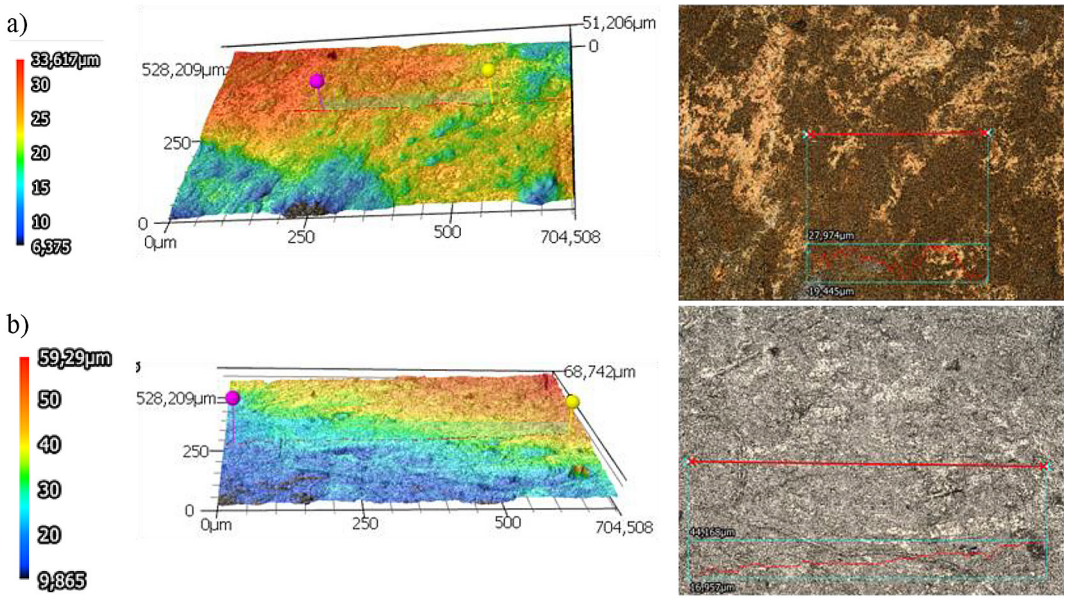

Figure 7. Surface structure of the selected cigarette sample: (a) filter tube (Ra= 0.112 µm, Rz= 0.424 µm), (b) tube for tobacco mixture (Ra= 0.117 µm, Rz= 0.66 µm)

understanding tribological mechanisms in conditions simulating the industrial process.

The roughness of the tread surface at the rounded edge of the profile, i.e. in the area of contact with the cigarette, was also determined. This test was carried out using two techniques: an optical profilometer, the VK-3100 Profilometer (described above), and a contact profilometer, the Surtronic S25 (Taylor Hobson Ltd., United Kingdom), which uses an inductive contact transducer with a diamond measuring tip (Figure 8).

The tests yielded roughness values of a similar nature, although slightly varied. These differences resulted from the difficulty in precisely placing the diamond needle of the profilometer exactly at the point of contact between the cigarette and the track. Therefore, particular attention was paid to the results of tests using a non-contact profilometer (Figure 9).

Methods

The measuring track (Figure 10) configured for determining the friction coefficient of selected types of tobacco products against the surface of the treadmill was constructed from a support frame, inside which an adjustable universal protractor was installed with an adjustable arm, along which there is a treadmill made of a 300 mm long Maker Beam XL aluminium profile.

This mechanism was installed on an MTS Insight 10 strength testing machine, which was used to force the set movement of the adjustable arm together with the treadmill. The position of the cigarette on the treadmill was precisely defined with an accuracy of 0.01 mm, which ensured the repeatability of individual tests.

The samples were placed sequentially on an aluminium track at the rounded edges of the upper

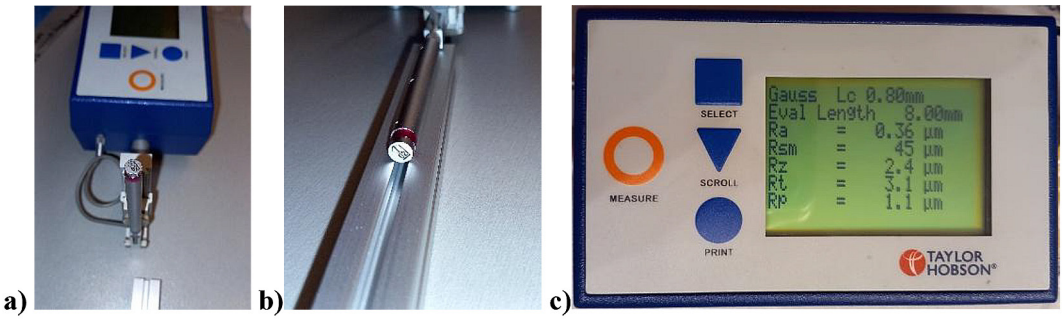

Figure 8. Testing the roughness of the treadmill surface on a Surtronic S25 profilometer, where: (a) profilometer before testing, (b) during testing, (c) display of the measuring device

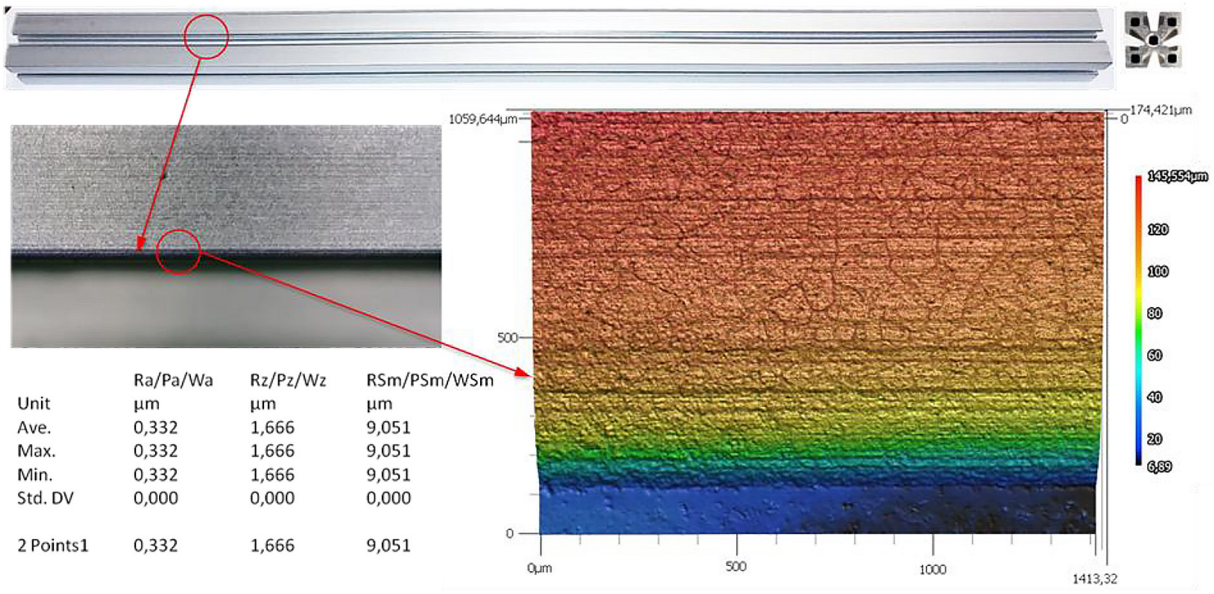

Figure 9. Surface structure of a tread fragment (Ra = 0.332 µm, Rz = 1.666 µm)

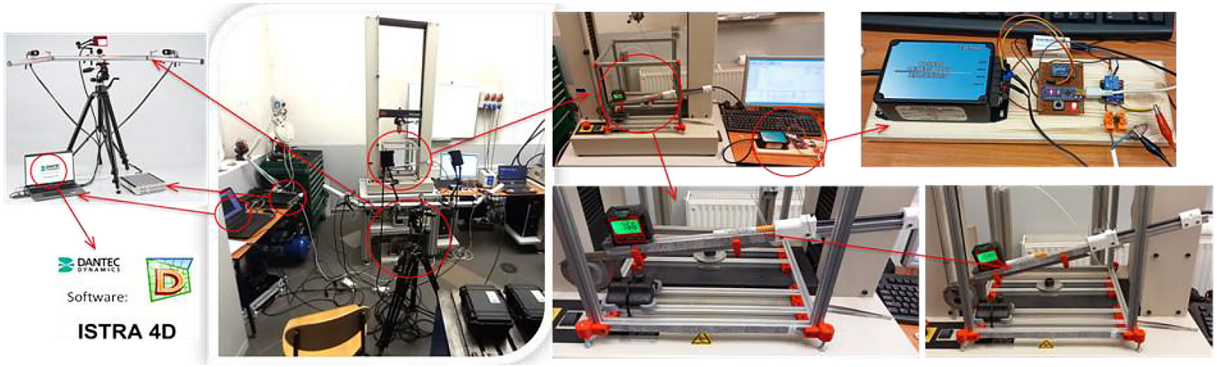

Figure 10. Structure of a measuring track for determining the friction coefficients of cigarettes

profile groove (Figure 11), and their displacement was recorded as the angle of inclination of the track was gradually increased. Speckles applied to the surface of the track, the samples and the levelled reference beam enabled accurate tracking of displacements in the Dantec Dynamics Istra4D module. The recorded angles of inclination at the moment the sample started moving were used to determine the coefficient of friction. The moment of motion initiation, corresponding to the breaking of static friction, was simultaneously recorded by a FiberOptic optical sensor located at the end of the treadmill, which allowed for precise correlation of data with displacements. To verify the accuracy and sensitivity of the system, reference measurements were performed using a steel roller with dimensions corresponding to the samples, characterised by a known coefficient of friction and roughness parameters. Each measurement was repeated multiple times, which made it possible to assess the repeatability and statistical reliability of the results and minimise the impact of sample variability and environmental factors. This experimental design ensured a reliable and quantitative analysis of the tribological behaviour of the tested fibre products.

The tests were conducted until the cigarette began to slide off the treadmill. Two independent measurement systems were responsible for observing the initiation of movement. The first measurement system was adapted to observe the displacement of the front of individual cigarettes. This system was created from a Fiberoptic RC171 displacement sensor (PHILTEC, INC., ANNAPOLIS, MD USA) and calibrated in such a way as to capture the initiation of movement of the samples with simultaneous signal and optical notification to the operator and the analyser in the second system. This made it possible to compare the responses of the individual measurement systems and verify the effectiveness of the tests. The second system, launched in parallel, is FlexDIC, a modular measurement system based on digital image correlation, consisting of three standard 5 Mpx CMOS cameras (2448 × 2048 px @ 24Hz) operating in GiGE technology, a central mounting bus, a set of lenses, calibration discs, a lighting system and a control unit with a laptop with Istra 4D software (Dantec Dynamics GmbH, Germany) and a DAQ controller. The three-camera configuration uses the so-called Central Reference Camera Perspective (CRCP), which increases the field of view and enables precise mapping of flat and curved surfaces. This system required the selection of a suitable matrix size with specs and the marking of samples by applying stochastically distributed markers around their perimeter (Figures 12 and 13).

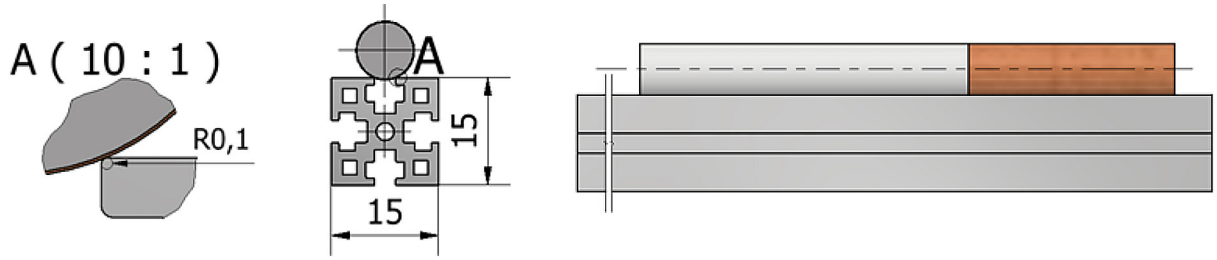

Figure 11. View of a cigarette placed on a tread forming the MakerBeam XL profile

Sample No.	Sample mass [g]	
	Before testing	After testing
1	0.729	0.730
2	0.705	0.706
3	0.707	0.708
4	0.732	0.733
5	0.723	0.725

Figure 12. View of 5 selected cigarette samples from 5 different packs with their corresponding weights obtained under humidity conditions of 55% after the conditioning process

The drawing of the physical model of the selected tobacco product sample placed on the treadmill illustrates the distribution of areas covered with specks. Area one (1) is the stationary base of the stand, serving as a reference level (levelling accuracy 0.05°). Area two (2) serves as a reference point on the moving treadmill with a cigarette, and area three covers the test sample. Detection of a change in the position of the straight line determined on the basis of selected points between areas two and three triggered the measurement of the angle between the line defined by the specula on the track and the level reference line.

The static friction coefficient (μ) was determined based on the angle φ shown in Figure 13. This angle corresponds to the point at which the static friction force is overcome and the sample begins to move. The value of μ was calculated as the tangent of the angle φ, which allows direct correlation between the precise measurements of displacements and deformations recorded by the digital image correlation (DIC) system and the value of the friction force. This approach ensures full transparency of calculations and allows the reader to follow the entire process - from displacement recording to obtaining the friction coefficient value. In order to further illustrate the procedure, a block diagram showing the successive stages of data processing and μ determination can be used.

RESULTS

This chapter presents the results obtained from tests carried out using the DIC system via the Istra 4D application, with parallel control of the Fiberoptic RC171 system (Figure 14).

The image shown (Figure 14) depicts a key stage of the tribological experiment, including the moment of initiation of the sample's movement relative to the raceway surface. The recording of image sequences in the DIC system enabled the precise determination of displacements and slip angles in relation to the axis of the system, while the Fiberoptic RC171 fibre optic sensor allowed for the unambiguous identification of the moment of static friction breakdown. The combination of data from both systems formed the basis for further analysis of the friction coefficient and

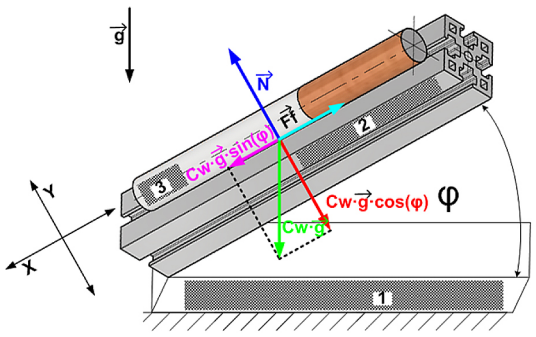

The force of friction F_f can be determined as:

$$F_f = \mu_s \cdot N$$

Where N and F_f can be calculated as:

$$N = C_w \cdot \cos\varphi \qquad F_f = C_w \cdot \sin\varphi$$

The coefficient of static friction can be calculated:

$$\mu_s = \frac{C \cdot \sin\varphi}{C \cdot \cos\varphi} = \tan\varphi$$

Figure 13. Physical model of friction between a tobacco product sample and a treadmill, where: Cw – Cigarette weight, Ff – Force of Friction, N – Normal Force, f – Incline angle

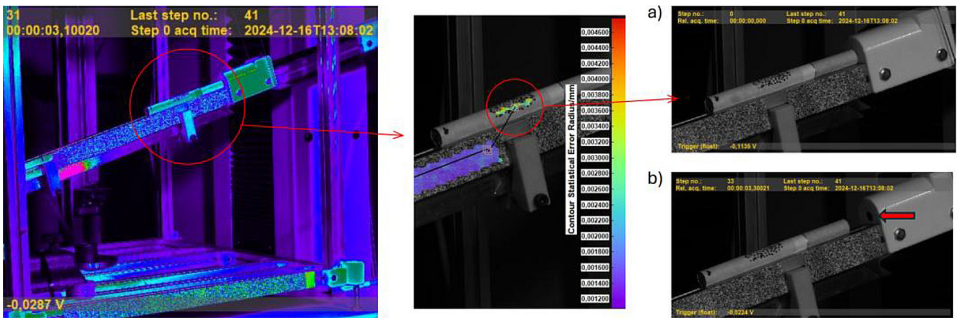

Figure 14. Tribological testing of a selected tobacco product: (a) view just before the initiation of movement, (b) view after the initiation of movement along the track (the red arrow indicates the front surface of the Fiberoptic RC171 optical sensor)

micro-movement characteristics at the contact point between the sample and the substrate.

The graph (Figure 15) shows the changes in the angle of inclination of the treadmill as a function of successive test steps. In the initial phase, a gradual, linear increase in the angle value is observed, corresponding to the stage of increasing inclination. The point marked on the graph corresponds to the moment of static friction breakdown, followed by the initiation of sample movement and the transition of the system to kinetic friction. The trend lines confirm the high repeatability of the curves and the precision of critical moment detection.

The graph (Figure 16) shows the characteristics of the angular rotation speed of the treadmill during the tribological test. The recorded oscillations are random and fall within the range of slight deviations from the average value, which confirms the high stability of the drive system and the precision of the inclination angle control during the measurement. The graph (Figure 17) shows the course of changes in the friction coefficient in successive steps of the experiment. The marked point corresponds to the moment of static friction breakdown, which is a key element of tribological analysis. The increase in the coefficient observed after the initiation of movement is secondary in nature and results from the dynamics of the system and the changing angle of the treadmill, without affecting the interpretation of the results in terms of static friction (Table 1).

The friction coefficient values for individual packages show moderate variability, ranging from 0.25 to 0.31. The lowest values were observed in samples from package No. 5, while the highest values were observed in package No. 1. The average friction coefficient for the entire population was 0.28 ± 0.028, which confirms the stability of the tribological properties of the tested materials under the adopted measurement conditions.

DISCUSSION

The proprietary research station included an angularly driven treadmill cooperating with a FiberOptic optical sensor and a drive control system, which allowed for precise mapping of the

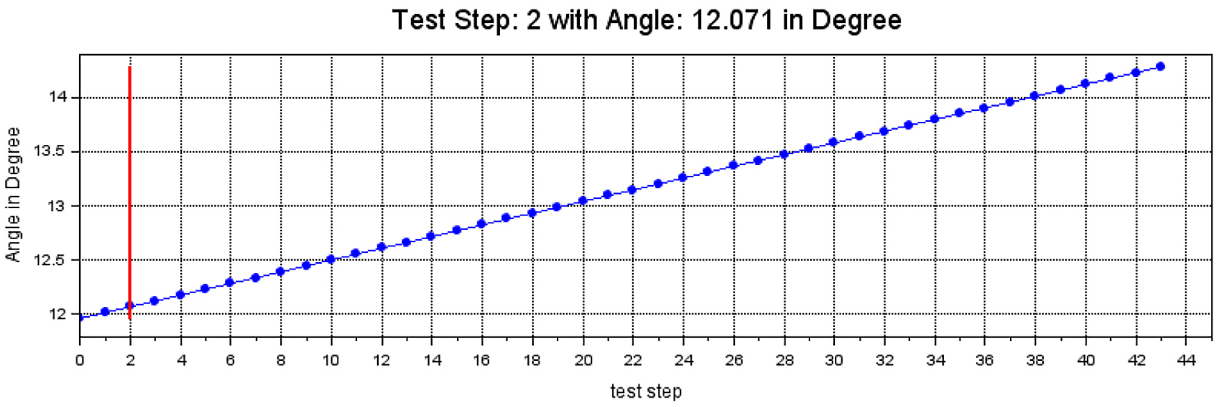

Figure 15. Results concerning angular displacements in the field of individual test steps

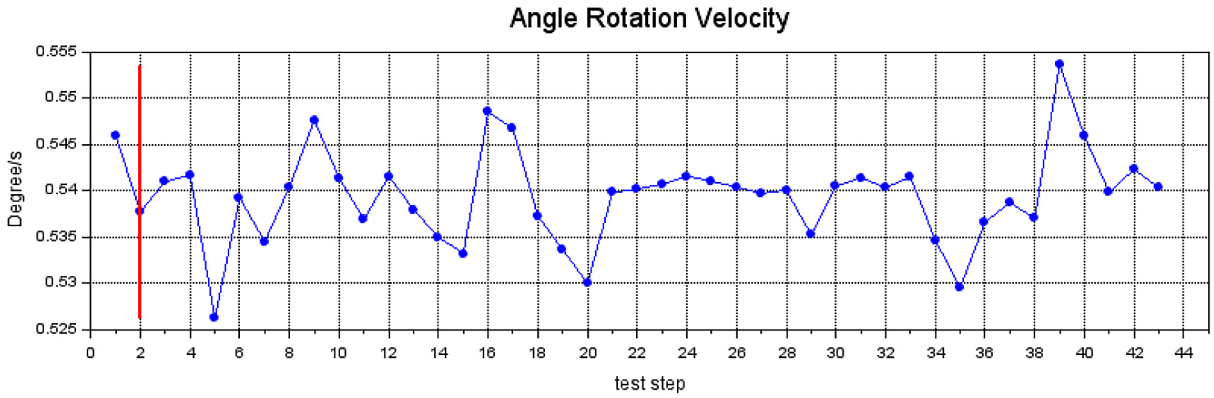

Figure 16. Characteristics of the angular rotation speed of the treadmill with the sample

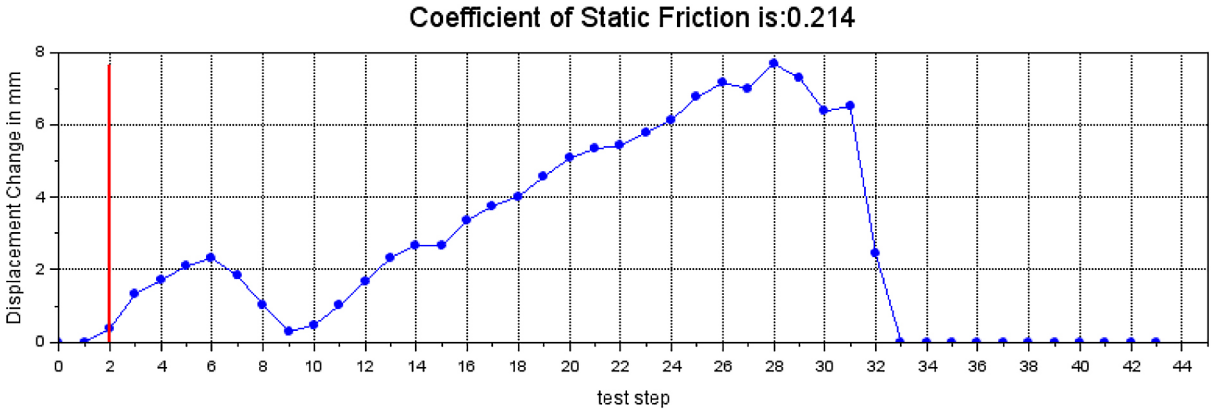

Figure 17. The course of the friction coefficient as a function of successive steps of the experiment, with the moment of static friction breaking marked

Table 1. Average friction coefficient values for five individual cigarette packs

Package number	Coefficient of friction	Standard deviation
1	0.3134	0.0323
2	0.3	0.0248
3	0.262	0.0335
4	0.2722	0.0244
5	0.2538	0.0237
Average results for the entire population	0.28	0.02774

moment of motion initiation and estimation of the forces acting during the actual production process. The integration of the stand with a digital image correlation system enabled the simultaneous acquisition of full-field data on the displacement and deformation of the tested parts under their own weight. The optical method used, employing Dantec Dynamics Istra4D software, allowed for high-resolution, non-contact measurements, which significantly increased the reliability and repeatability of tribological analyses.

The surface roughness of the tested fibrous products and the reference sample was characterised. The measurement of topographical parameters, such as Ra and Rz, enabled the assessment of the surface microgeometry and its potential impact on friction and contact interactions. For each category of samples, a set of tables and graphs was prepared, which enabled a comparison of the surface roughness properties of individual tobacco products. Analysis of these data enabled an assessment of the influence of surface microstructure on tribological mechanisms, with particular emphasis on the differences between fibrous materials. When analysing the results obtained, it is important to link the friction coefficient to the microgeometry of the surface, as determined in the course of surface testing. From a tribological point of view, surface roughness affects friction through:

- contact interactions at the microscopic level – peaks of irregularities (asperities) generate

local contact points between the fibres and the running surface, increasing friction resistance,
- adhesion and elastic deformation mechanisms – greater roughness can increase mechanical contact and local stresses, which translates into higher friction coefficients,
- extension of the friction path – surfaces with high topography make the contact surface more complex, which increases the total resistance when moving the sample.

CONCLUSIONS

The study highlights the crucial role of tribological properties of fibrous materials in the efficiency and reliability of tobacco product manufacturing processes. The experimental approach demonstrated that precise determination of frictional interactions can inform improvements in production stability and continuity. Key conclusions are as follows:

- Friction between cigarette materials and production equipment is a major factor influencing process efficiency and stability.
- Surface roughness and fibre structure significantly affect tribological behaviour and should be considered in process optimisation.
- The methodology applied provides detailed insights into subtle material interactions and can inform both material selection and equipment design.
- The approach has potential applicability beyond the tobacco industry, particularly in packaging sectors involving transport, positioning, or separation of light fibrous products or films.
- Further research should explore the influence of fibre microstructure and environmental conditions such as humidity and temperature, as well as extend the methodology to other fibrous materials to fully characterise tribological behaviour.

REFERENCES

1. Gupta B. S., El Mogahzy Y. E., Friction in fibrous materials: Part I: Structural model: Part I: structural model. Textile Research Journal. 1991;61(9):547–555. https://doi.org/10.1177/004051759106100907
2. El Mogahzy Y.E., Gupta B. S., Friction in fibrous materials: Part II: experimental study of the effects of structural and morphological factors: Part II: experimental study of the effects of structural and morphological factors. Textile Research Journal. 1993;63(4):219–230. https://doi.org/10.1177/004051759306300405
3. Ward A., Hilitski F., Schwenger W. et al., Solid friction between soft filaments. Nature Mater 2015;14:583–588. https://doi.org/10.1038/nmat4222
4. Prusinowski, A., Kaczyński, R. (2020). Tribological behaviour of additively manufactured fiber-reinforced thermoplastic composites in various environments. Polymers, 12. https://doi.org/10.3390/polym12071551
5. Johansson, P., Marklund, P., Björling, M., Shi, Y. Effect of humidity and counterface material on the friction and wear of carbon fiber reinforced PTFE composites. Tribology International, 2021;157:106869. https://doi.org/10.1016/j.triboint.2021.106869
6. Arcifa, A., Rossi, A., Espinosa-Marzal, R., Spencer, N. Influence of environmental humidity on the wear and friction of a silica/silicon tribopair lubricated with a hydrophilic ionic liquid. ACS applied materials & interfaces, 2016;8 5:2961–73. https://doi.org/10.1021/acsami.5b09370
7. Chen, Z., He, X., Xiao, C., Kim, S. Effect of humidity on friction and wear—a critical review. Lubricants. 2018. https://doi.org/10.3390/lubricants6030074
8. Randhawa, K., Patel, A. The effect of environmental humidity/water absorption on tribo-mechanical performance of polymers and polymer composites – a review. Industrial Lubrication and Tribology. 2021. https://doi.org/10.1108/ilt-02-2021-0045
9. Luo, M., Huang, S., Man, Z., Cairney, J., Chang, L. Tribological behaviour of fused deposition modelling printed short carbon fibre reinforced nylon composites with surface textures under dry and water lubricated conditions. Friction, 2022;10:2045–2058. https://doi.org/10.1007/s40544-021-0574-5
10. Dhakal, N., Espejo, C., Morina, A., Emami, N. Tribological performance of 3D printed neat and carbon fiber reinforced PEEK composites. Tribology International. 2024. https://doi.org/10.1016/j.triboint.2024.109356
11. Shim, H., Kwon, O., Youn, J. Effects of fiber orientation and humidity on friction and wear properties of graphite fiber composites. Wear, 1992;157:141–149. https://doi.org/10.1016/0043-1648(92)90192-b
12. Johansson, P., Marklund, P., Björling, M., Shi, Y. Mechanisms behind the environmental sensitivity of carbon fiber reinforced polytetrafluoroethylene (PTFE). Friction, 2023;12:997–1015. https://doi.org/10.1007/s40544-023-0824-9
13. Negi V., Picu R. C. Mechanical behavior of nonwoven non-crosslinked fibrous mats with adhesion and friction Soft Matter, 2019;15:5951–5964. https://doi.org/10.1039/C9SM00658C

14. Wilbrink D.V., Beex L.A.A., Peerlings R.H.J., A discrete network model for bond failure and frictional sliding in fibrous materials, International Journal of Solids and Structures, 2013; 50(9):1354–1363, https://doi.org/10.1016/J.IJSOLSTR.2013.01.012
15. Nurhidayah Ismail, Matthijn B. de Rooij, Erik G. de Vries, Nurul Hilwa Mohd Zini, Dik J. Friction between single aramid fibres under pretension load, Schipper, Tribology International, 2019;137: 236:245, https://doi.org/10.1016/J.TRIBOINT.2019.04.013
16. Luo L., Stylios G., A review of friction in low-stress mechanics of fibrous flexible materials. Materials, 2024;17:3828. https://doi.org/10.3390/ma17153828
17. Shen, Y., Buslovich, D.G., Panin, S.V., Kornienko, L.A., Dobretsov, P.V., Kolobov, Y.M. Tribological characteristics of fibrous polyphthalamide-based composites. Polymers 2024;16:2274. https://doi.org/10.3390/polym16162274
18. Chen Q., Yan X., Chen K., Feng C., Wang D., Li X., Zhao X., Chai Z., Wang Q., Zhang D., Zeng H., Electrospun fibrous membrane reinforced hydrogels with preferable mechanical and tribological performance as cartilage substitutes, Journal of Materials Chemistry, 2023;11:1713–1724. https://doi.org/10.1039/D2TB02511F
19. Kan W. H., Albino C., Dias-da-Costa D., Dolman K., Lucey T., Tang X., Cairney J., Proust G., Fracture toughness testing using photogrammetry and digital image correlation, MethodsX, 2018;5:1166–1177. https://doi.org/10.1016/j.mex.2018.09.012
20. Tan J. Y., Chow Sai Kit A., Tan C. W., Sentiment Analysis on Game Reviews: A Comparative Study of Machine Learning Approaches, International Conference on Digital Transformation and Applications (ICDXA), 25–26 October 2021;209–216. https://doi.org/10.56453/icdxa.2020.1009.10
21. Goh C. P., Mani M. R., Scanner-Based Digital Image Correlation Method for Mechanical Characterization of Rubber, International Conference on Digital Transformation and Applications (ICDXA) 2020, 2020;95–99, https://doi.org/10.56453/icdxa.2020.1009
22. Abdulqader A., Rizos D. C., Advantages of using digital image correlation techniques in uniaxial compression tests, Elsevier, Results in Engineering, 2020;6:100109, https://doi.org/10.1016/j.rineng.2020.100109
23. Kan W. H., Albino C., Dias-da-Costa D., Dolman K., Lucey T., Tang X., Cairney J., Proust G., Fracture toughness testing using photogrammetry and digital image correlation, Elsevier, MethodsX, 2018;5:1166–1177. https://doi.org/10.1016/j.mex.2018.09.012
24. Karimi J., Nejati H. R., Ahmadi M., Application of digital image correlation to derive Paris' law constants in granite specimens, Elsevier, Theoretical and Applied Fracture Mechanics, 2023;128:104166, https://doi.org/10.1016/j.tafmec.2023.104166
25. Schreier, H.W., Sutton, M.A. Systematic errors in digital image correlation due to undermatched subset shape functions. Experimental Mechanics 2002;42:303–310. https://doi.org/10.1007/BF02410987 https://doi.org/10.1007/BF02410987
26. Yan Z., Dai F., Liu Y., Wei M., You W., New insights into the fracture mechanism of flattened Brazilian disc specimen using digital image correlation, Elsevier, Engineering Fracture Mechanics, 2021;252:107810, https://doi.org/10.1016/J.ENGFRACMECH.2021.107810
27. Tabiai I., Tkachev G., Diehl P., Frey S., Ertl T., Therriault D., Lévesque M., Hybrid image processing approach for autonomous crack area detection and tracking using local digital image correlation results applied to single-fiber interfacial debonding, Elsevier, Engineering Fracture Mechanics, 2019;216:106485, https://doi.org/10.1016/j.engfracmech.2019.106485
28. Amjad K., Christian W.J.R., Dvurecenska K., Chapman M.G., Uchic M.D., Przybyla C.P., Patterson E.A., Computationally efficient method of tracking fibres in composite materials using digital image correlation, Elsevier, Composites Part A: Applied Science and Manufacturing, 2020;129:105683, https://doi.org/10.1016/j.compositesa.2019.105683
29. Goh C. P., Mani M. R., Scanner-Based Digital Image Correlation Method for Mechanical Characterization of Rubber, International Conference on Digital Transformation and Applications (ICDXA) 2020;95–99, https://doi.org/10.56453/icdxa.2020.1009
30. Ward, A., Hilitski, F., Schwenger, W. et al. Solid friction between soft filaments. Nature Mater 2015;14:583–588, https://doi.org/10.1038/nmat4222
31. Shen Y., Buslovich D.G., Panin S.V., Kornienko L.A., Dobretsov P.V., Kolobov Y.M., Tribological Characteristics of Fibrous Polyphthalamide-Based Composites. Polymers 2024;16:2274. https://doi.org/10.3390/polym16162274
32. Ismail N., de Rooij M. D., de Vries E. G., Zini N. H. M., Schipper D. J., Friction between single aramid fibres under pre-tension load, Tribology International, 2019;137:236–245, https://doi.org/10.1016/j.triboint.2019.04.013
33. Sevostyanov, P.A., Samoilova, T.A., Tikhomirova, M.L. Dry and viscous friction, statistical factors, fluctuation-dissipation theorem and features of their manifestations in relaxation of fibrous materials. Fibre Chem 2020;51;449–451. https://doi.org/10.1007/s10692-020-10131-8